


RESEARCH ARTICLE | OCTOBER 06 2023

Model predictive assistance for operational decision making in molten salt receiver systems

Christian Schwager ; Florian Angeley; Peter Schwarzbözl; Cristiano José Teixeira Boura; Ulf Herrmann



AIP Conf. Proc. 2815, 030020 (2023)

<https://doi.org/10.1063/5.0151514>



View
Online



Export
Citation

CrossMark



APL Energy

Latest Articles Online!

Read Now



Model Predictive Assistance for Operational Decision Making in Molten Salt Receiver Systems

Christian Schwager^{1, a)}, Florian Angele^{1, b)}, Peter Schwarzbözl^{2, c)}, Cristiano José Teixeira Boura^{1, d)}, Ulf Herrmann^{1, e)}

¹ Solar-Institut Jülich of, FH Aachen University of Applied Sciences (SIJ), 52428 Jülich, Germany

² Institute of Solar Research, German Aerospace Center (DLR), 51170 Köln, Germany

^{a)} Corresponding author: schwager@sj.fh-aachen.de

^{b)} angele@sj.fh-aachen.de

^{c)} peter.schwarzboezl@dlr.de

^{d)} boura@sj.fh-aachen.de

^{e)} ulf.herrmann@sj.fh-aachen.de

Abstract. Despite the challenges of pioneering molten salt towers (MST), it remains the leading technology in central receiver power plants today, thanks to cost effective storage integration and high cost reduction potential. The limited controllability in volatile solar conditions can cause significant losses, which are difficult to estimate without comprehensive modeling [1]. This paper presents a Methodology to generate predictions of the dynamic behavior of the receiver system as part of an operating assistance system (OAS). Based on this, it delivers proposals if and when to drain and refill the receiver during a cloudy period in order maximize the net yield and quantifies the amount of net electricity gained by this. After prior analysis with a detailed dynamic two-phase model of the entire receiver system, two different reduced modeling approaches were developed and implemented in the OAS. A tailored decision algorithm utilizes both models to deliver the desired predictions efficiently and with appropriate accuracy.

INTRODUCTION & MOTIVATION

Operating a molten salt tower (MST) is challenging due to strict temperature limitations of the heat transfer medium and the complexity of this system. Depending on the current mass flow rate, the molten salt usually takes between one and ten minutes to pass through the receiver. Therefore, conventional feedback and feedforward controllers struggle to stabilize the outlet temperature in volatile radiation conditions [2]. Even sophisticated model predictive controllers, which can achieve much higher control quality, need to decrease the outlet temperature in certain situations to prevent local hot spots [1], which is a phenomenon caused by alternating shading that only affects a portion of the heliostat field. Therefore, commercial plant operators usually do not react to cloud passages by mass flow adaptation of the external molten salt receiver. Instead, the mass flow is maintained to prevent local hot spots and consequently allow outlet temperatures to drop significantly [3].

In general, these outlet temperature variations affect the exergy provided by the warm/hot molten salt flow and consequently deteriorates the heat-to-power conversion efficiency. Whenever the outlet temperature is too low and the molten salt must be recycled into the cold storage tank, it draws further losses with it. To illustrate these effects, Figure 1 (b) depicts the nominal molten salt flow pattern, where the hot mass flow coming from the receiver is charged into the hot storage tank, while the steam generator (power block) feeds from the hot storage tank and returns the cooled molten salt into the cold storage tank. Assuming a nearly nominal return temperature of the steam generator, the medium temperature in the cold storage tank would stay constant, since thermal losses are usually negligible in commercial molten salt storages of this scale. As long as solar conditions do not change, net efficiency parameters such as receiver efficiency η_{rec} and pumping power P_{pumps} stay constant as well. Depending on the difference between

the current hot storage tank medium temperature and the one of the incoming mass flow, the first varies more or less and therefore affects the heat-to-power efficiency of the power block η_{PB} .

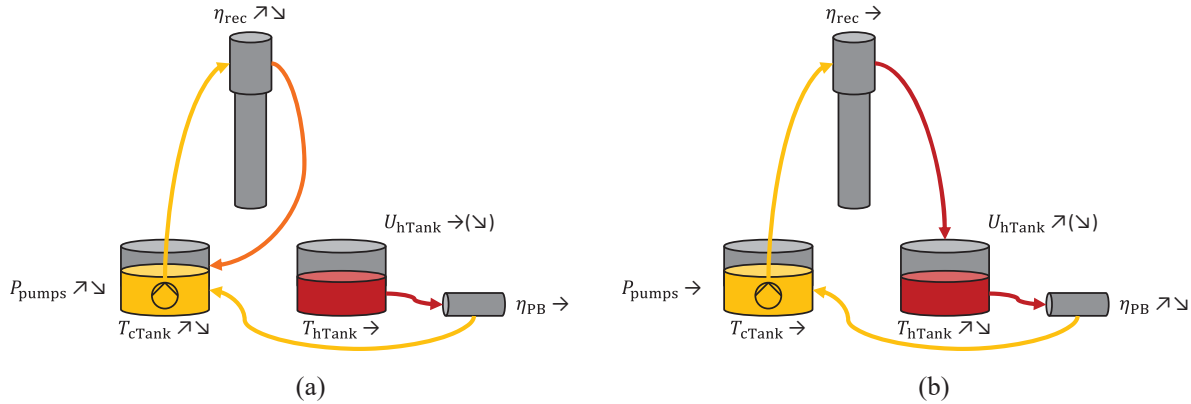


FIGURE 1. Comparison of molten salt recycling (a) vs. storage charging mode (b) and their effects on different components of receiver and storage system of a MST

Since the steam generator cannot handle large feed temperature variation, the hot molten salt mass flow from the receiver must be recycled into the cold storage tank, whenever it falls below a certain threshold, as shown in Figure 1 (a). In this case, the medium temperature of the cold storage tank varies instead. Most likely, the incoming flow is hotter than the inventory of the cold storage tank and can cause a significant temperature rise. Only if the receiver is operated at very low incidence flux it acts as a radiator and therefore cools down the cold storage tank inventory. As a result, the pumping power P_{pumps} varies, because the receiver mass flow needs adjustment to maintain the same (clear-sky) outlet temperature. Since the inlet temperature affects the average receiver surface temperature, the receiver efficiency η_{rec} also varies with the cold storage temperature. This phenomenon does not have an instantaneous effect, but instead it gradually affects the net efficiency of future operation. E.g. if the cold storage temperature rises over a certain period, the net efficiency will be impaired for the subsequent operation until the cold storage temperature normalizes again.

The above described effects and the fact that in cloudy conditions auxiliary losses stay high, lead to the question if and when it might be beneficial to temporarily drain and refill the receiver in order to minimize energy losses and increase the net electricity yield. Making this decision during operation poses a challenging task, since transitioning a molten salt receiver system from one to another operating state requires certain steps and respective time. This causes other energy losses, which need to be weighed against the losses we are trying to avoid.

Figure 2 gives an overview of the basic operating states and transition for the receiver system considered in this work. (compare [4]). The dark arrows indicate transitions of the daily startup (upper) and shutdown (lower) procedure. The startup includes more transitions due to the startup delay of the receiver pumps and the need to preheat the absorber tubes prior to flooding. For safe operation during cloudy conditions, the system can switch from “Normal Operation” into “Filled Cloud Protection” transitioning from temperature feedback control to (semi fixed) clear-sky mass flow control. The above-discussed maneuver of temporarily draining the external receiver during cloudy conditions relates to the transitions in light grey arrows, which lead into the operating state “Drained Cloud Protection”. In this state, the receiver panels are fully drained and usually cool down due to external heat losses and insufficient solar radiation. The pumps slow down to minimum mass flow saving parasitic energy consumption. From there control system can transition into “Preheat” state and follow the remaining transitions of the daily startup procedure in order to restart heat production.

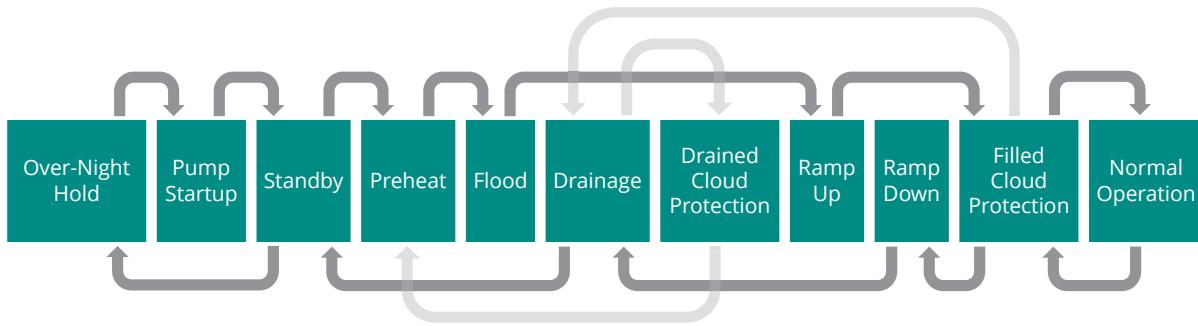


FIGURE 2. Operating states and transitions of the considered molten salt receiver system (without special and emergency transition)

Model predictive assistance can help to make an optimal decision in situations when it is not obvious whether continuing operating through a cloudy period or temporarily draining the receiver would yield higher net outcome. This paper presents a methodology for identifying such cases and determining the optimal time for a temporary drainage based on predicted net yield taking into account the relevant dynamic effects. As part of an operating assistance system (OAS), it generates decision proposals based on dynamic simulation and analysis and quantifies the expected benefit from a proposed maneuver.

METHODOLOGY

As a basis for the development of the OAS and later validation, a detailed dynamic process model of the receiver system including thermal storage has been developed and validated by CFD/FEM simulations as well as experimental data [5]. It includes a two-phase (2P) fluid and flow model to realistically mimic temperature development in the absorber tubes during flood and drainage simulations. Combined with a discretization of the absorber tube – two elements in circumferential and a variable number of elements in vertical direction – it realistically represents the dynamic behavior of the controlled receiver system and calculates local temperatures in the fluid as well as on inner and outer tube surfaces. This model also incorporates all operating states and transitions as presented in Figure 2.

Since the discussed application requires a method to generate a process prediction and derive an optimal decision within minutes, the OAS applies reduced models, as depicted in Figure 3, which are deduced from and validated by the detailed dynamic 2P model. As illustrated on the right hand side, the detailed dynamic 2P model was introduced for the development, but is not part of the actual functionality of the OAS. The Flux input (on the left) is provided by a Raytracing Software [6], which converts spatial DNI forecast data into a series of predicted receiver flux distribution maps.

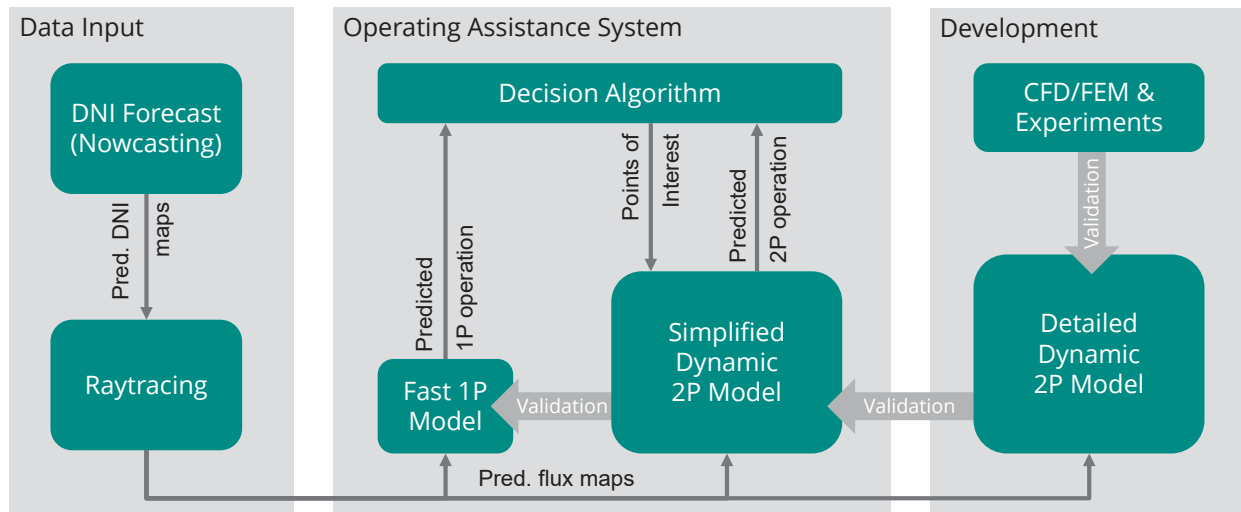


FIGURE 3. Basic illustration of the different components and data flow in the OAS

First, a fast single-phase (1P) model simulates the normal operation to predict temperature trends and net yield for a hypothetical continuous operation over a large prediction window. A **decision algorithm** is implemented to analyze these results and identify points, which indicate energy saving potential by temporary drainage (more details in Results and discussion). It then triggers a simplified dynamic 2P model to simulate an isolated sequence of draining and refilling according to the transitions described above. By comparing the results of the two different simulations – continuous operation with the fast 1P model and temporary drainage with the simplified dynamic 2P model – the decision algorithm determines the difference in net yield over the relevant period. If the predicted net yield is significantly greater with temporary drainage than with continuous operation, the OAS recommends this maneuver to the operator.

By utilizing models reduced to different degrees, the OAS combines their strengths. The **fast 1P model** primarily serves the purpose for the decision algorithm, which is to determine the trend of the system's net power quickly. It comprises a semi-steady-state receiver model, a dynamic storage model and model for the receiver pumps. The receiver model includes a scalar steady state energy balance, considering convective and conductive heat flow as well as external losses through reflection, convection and radiation. By applying a second order delay to the receiver outlet temperature, this receiver model has a dynamic behavior similar to the fully dynamic models. Further, one dynamic energy and mass balance for each tank represents the storage model and the pump model determines the pumping power by a given efficiency and prescribed mass flow. This model does not represent any hydraulic equations, hence the fast computing performance.

In contrast, the **simplified dynamic 2P model** is a reduced derivative from the detailed dynamic 2P model [5]. The included receiver model has a reduced vertical discretization and panels that are connected in parallel, are not modelled individually. Instead, each vertical pass is represented by one absorber tube model with a corresponding fraction of the mass flow rate and (horizontally) averaged solar flux. As shown in Table 1, the complexity of this model differs from the fast 1P model by nearly two orders of magnitude, which is also due to the 2P feature of the implemented fluid flow model. This is required to realistically simulate drain and refill procedures. Consequently, the same comprehensive process control system is implemented as in the detailed model, including the transition according to Figure 2. Analogously, the simplified dynamic 2P model comprises all relevant periphery components, such as control valves, drain and vent valves, piping, pumps, buffer vessels and storage tanks. Additionally, the initialization of the simplified model is modified so that the simulation can start at any time of a scenario. This saves valuable computing time, since the OAS only requires the 2P model to simulate a designated time window.

TABLE 1. Comparison of the different process models

	Fast 1P Model	Simplified Dynamic 2P Model	Detailed Dynamic 2P Model
Two-phase fluid model	No	Yes	Yes
Discrete rec. elements	1	36	102 – 408
Time varying states	~500	~10,000	~20,000 – 50,000
Differentiated variables	~10	~700	~1,500 – 4,000

Both, the fast 1P model and the simplified dynamic 2P model include the same virtual net power approach. Since the molten salt thermal storage decouples the electricity production schedule from the solar part respectively the receiver system, it is not necessary to model the performance of the power block. Instead, the obtained net power P_{net}^* represents the net electricity that can be produced by the power block from the thermal energy provided by the receiver excluding associated losses. The temperature dependence of the heat-to-power efficiency η_{PB} can be taken into account by considering the exergy, because in the relevant temperature regime the exergy efficiency of a typical power block ζ_{PB} can be assumed to be constant. In this sense, each model calculates the rate at which the exergy content changes in the hot storage tank plus the exergy flow that is currently fed to the steam generator and converts it into net power by multiplication with the exergy efficiency ζ_{PB} and subtraction of parasitic losses P_{pumps} .

$$P_{\text{net}}^* = \left[\frac{d(\Delta E_{\text{x,hTank}})}{dt} + \Delta \dot{E}_{\text{→SG}} + (\Delta \dot{E}_{\text{→cTank}} - \Delta \dot{E}_{\text{loss}}^*) \right] \cdot \zeta_{\text{PB}} - P_{\text{pumps}} \quad (0.1)$$

The difference in parentheses additionally accounts for recycled molten salt (when the outlet temperature is low), which is subject to indirect losses $\Delta \dot{E}_{\text{loss}}^*$. I.e. losses that are caused by current operating parameters but which will

occur later (outside of the investigated prediction interval). More comprehensive details about the derivation of the virtual net power approach and the modelling mentioned above, is prepared to be published soon.

In order to test the OAS in a simulation environment, the models are parameterized to a hypothetical plant site in South Africa. The considered layout of the 650 MW_{th} receiver system originates from a development by General Electric including an external cylindrical receiver with two parallel flow paths operated in serpentine flow [4]. The tower is approx. 200 m high and the surrounding heliostat field is optimized by using of the tool HFLCAL [7]. The aim point configuration is optimized considering allowable flux density limits and film temperature limits using an ant colony optimization algorithm [8].

RESULTS AND DISCUSSION

The following results demonstrate the functionality of the above described assistance feature by means of a test scenario. Figure 4 shows an image plot of the flux input which the OAS receives from the raytracing software. In this method of illustration, the two-dimensional discretization of the cylindrical receiver (vertically along the tubes and horizontal for each panel) is flattened into a single column. Every six rows of pixels represent one panel. The top and bottom of the plot represents northerly oriented panels and the centerline the southern side of the receiver. This allows observing local shadings on the receiver as well as an indication for the direction of their movement. In the given scenario, the c-shaped patterns reveal that these clouds cross the plant from south to north. However, more obvious is the heavy cloud coverage for approximately one hour in the middle of the displayed period, which is subject of this test.

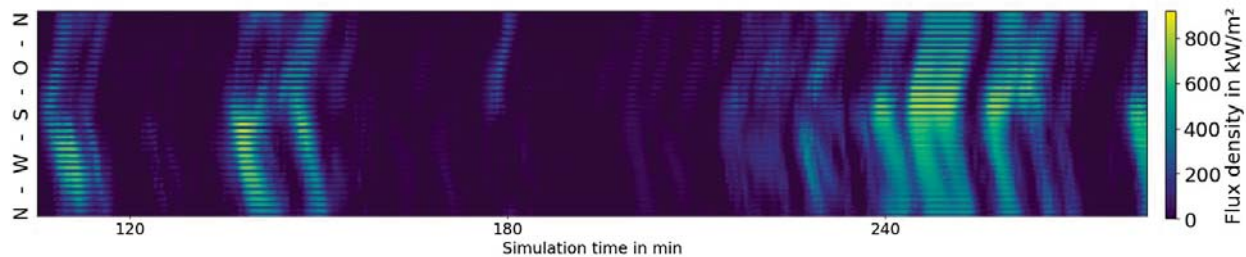


FIGURE 4. Receiver flux densities of the test scenario plotted over time

In order to determine, whether continuous or interrupted operation with draining and refilling the receiver yields more net energy, the OAS first runs a prediction on the fast 1P model resulting in the black graphs in Figure 5 and Figure 6. According to this prediction the net power drops down to below -10 MW_{el} , even though the corresponding parasitic losses are only approx. 4 MW_{el} . Hence, 60 % of this net energy loss is due to thermal losses as the receiver effectively draws energy from the thermal storage, when the receiver outlet temperature undercuts the inlet temperature. It is worth mentioning, that these values apply to only one flow path (half of the cylindrical receiver). The other flow path shall be handled separately, since they can be operated and controlled independently from each other. This allows numerical parallelization to achieve shorter computing times.

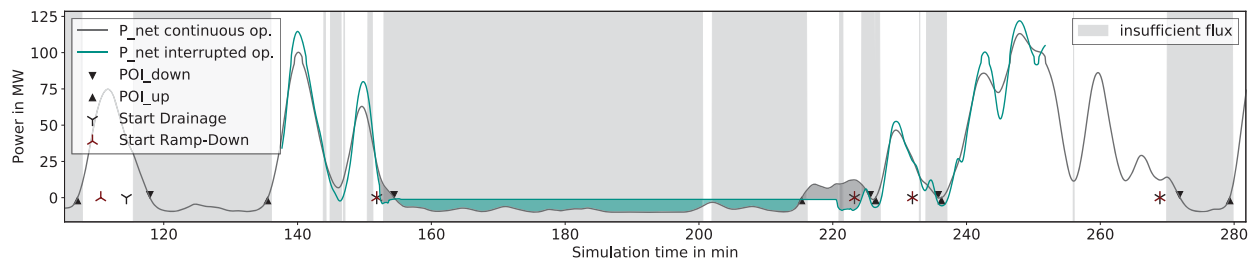


FIGURE 5. Predicted net power trends and results of the decision algorithm for a POI with positive net benefit

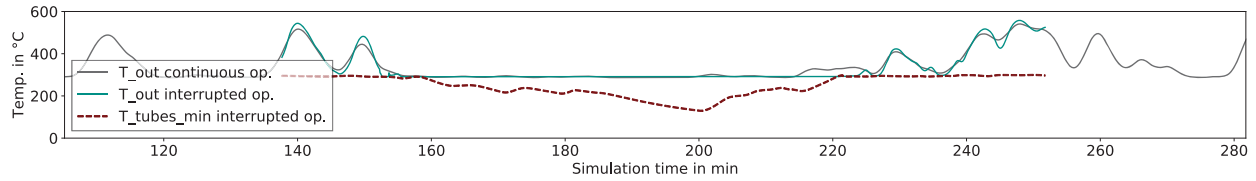


FIGURE 6. Predicted trends of the receiver outlet temperature and the minimum of all measured tube (backside) temperatures in the test scenario

Based on these results the decision algorithm identifies points of interest (POI), which mark the period of negative net power. Ideally, the system would harvest all of the positive net power and start the drainage at exactly the POI_{down} . Nevertheless, to avoid any risk of freezing salt during drainage, a certain amount of solar flux is required to keep the absorber tube warm until drainage is completed. Therefore, the decision algorithm determines for each receiver panel individually when there is sufficient flux available to counteract radiation and convection losses at drainage temperature. As a result, the grey shading in Figure 5 marks all time steps at which this condition is not given for at least one panel of the considered flow path. Since in the displayed period, all POI_{down} are at times of insufficient flux, accordingly the corresponding starting points of the drainage (black asterisks) are each placed earlier and with a certain distance to the edge of the grey shading to account for the drainage duration of approx. 60 s.

Finally, the decision algorithm determines when the transition should be initiated. Prior to drainage the outlet temperature of the external receiver needs to be ramped down at a certain rate, in order to avoid rapid cooling of the empty absorber tubes. Therefore, the algorithm determines each starting point (red asterisks) by an intersection of the prescribed temperature ramp and the temperature trend of the continuous operation. This information is then transferred to the simplified dynamic 2P model, which simulates the drainage and refill procedure regarding one pair of POI_{down} and POI_{up} .

The results are shown by the green graphs in Figure 5 and Figure 6. As expected, the net power of the drained system is almost zero, thanks to the minimal pumping energy loss and eliminated thermal receiver losses. Nevertheless, there is a noticeable deficit during the drainage compared to the continuous operation. Especially after the continuous operation returns to positive net power, it takes 9.5 min for the interrupted operation to catch up onto the same level, resulting in significant amounts of unharvested solar energy being lost. Figure 6 reveals, that the absorber tubes cool down quite far so the receiver system needs a while to preheat before the receiver panels can be flooded with molten salt again.

However, the net benefit resulting from the difference between the dark-grey and green areas in Figure 5, is +4.8 MW_{el} . Hence, temporary drainage is recommended in this case. In contrast, the net benefit of temporary drainage is negative one POI earlier, as it can be seen in Figure 7. This is due to the great amount of unharvested solar energy right after the shading. This indicates that the net benefit is highly sensitive to how quick shading disappears in relation to the time it takes to reheat and refill the absorber tubes.

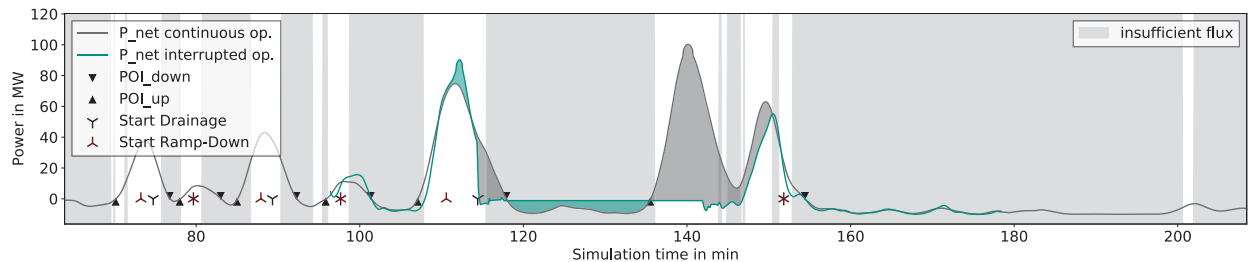


FIGURE 7. Predicted net power trends and results of the decision algorithm for a POI with negative net benefit

CONCLUSION & OUTLOOK

With the objective to increase operational efficiency of a molten salt tower (MST) plant, a model predictive feature for an operating assistance system (OAS) has been developed and successfully tested. It utilizes multiple models, which are reduced to different degrees, in order to maximize computing performance while maintaining reasonable representation of the complex system. With help of two-phase modelling and comprehensive control system

implementation, the OAS can predict realistically the net power of the receiver system equivalent to electricity production and proposes an optimal timing for temporary drainage in case of positive net benefit of this maneuver as well as a quantification of the latter.

The test scenarios that have been analyzed so far, indicate that it will be challenging to derive a general conclusion about when a temporary drainage would be more efficient. It is obvious that the answer depends on the degree of shading and the duration of this event. However, it can be observed that there is also a high sensitivity to how fast the shading disappears, which relates to the characteristic of the cloud edges and cloud velocity. However, the direction of cloud movement is relevant, since cloud moving in latitudinal direction can cover the heliostat field portion supplying one flow path twice as fast as when moving in longitudinal direction. Depending on these conditions, the allowed rate at which the outlet temperature is ramped up after refilling has more or less effect on how much yield is lost by this maneuver. This complexity underlines the value of an OAS with features like the one presented in this paper.

A more in-depth analysis of the sensitivities as well as detailed validation of the reduced model will follow in further publications. In addition, tests with actual DNI-prediction data from current now-casting systems are subject of current research in order to derive the required quality of input data and to compare observations with synthetic clouds to those with real cloud shapes and movements.

ACKNOWLEDGMENTS

The authors gratefully acknowledge the financial support by the German Federal Ministry for Economic Affairs and Energy (BMWi).

REFERENCES

1. C. Schwager, C. J. T. Boura, R. Flesch, S. Alexopoulos, and U. Herrmann, [AIP Conference Proceedings](#) **2126**, 30054 (2019).
2. R. Flesch, D. Maldonado, and P. Schwarzbözl in *9th Mathmod Conference 2018* (2018).
3. S. Relloso, *Noor III 150 MW Molten Salt Tower: 1st Year of Commercial Operation* (Casablanca, 2019).
4. A. K. Das, P. Iñigo, R. J. Terdalkar, A. Joshi, C. Wang, M. M. Clark, D. McGrane, and L. Deng, [Energy Procedia](#) **69**, 350 (2015).
5. C. Schwager, R. Flesch, P. Schwarzbözl, U. Herrmann, and C. J. Teixeira Boura, Manuscript submitted for publication (2021).
6. N. Ahlbrink, B. Belhomme, R. Flesch, D. M. Quinto, A. Rong, and P. Schwarzbözl, “STRAL. Fast Ray Tracing Software With Tool Coupling Capabilities for High-Precision Simulations of Solar Thermal Power Plants,” in *Proceedings of the SolarPACES Conference 2012* (2012).
7. P. Schwarzbözl, R. Pitz-Paal, and M. Schmitz in *SolarPACES Conference 2009* (2009).
8. R. Flesch, C. Frantz, D. Maldonado Quinto, and P. Schwarzbözl, [Solar Energy](#) **155**, 1273 (2017).